



# CHORUS

This is the accepted manuscript made available via CHORUS. The article has been published as:

## Detailed spectroscopy of $^{110}\text{Cd}$ : Evidence for weak mixing and the emergence of $\gamma$ -soft behavior

P. E. Garrett *et al.*

Phys. Rev. C **86**, 044304 — Published 1 October 2012

DOI: [10.1103/PhysRevC.86.044304](https://doi.org/10.1103/PhysRevC.86.044304)

# Detailed spectroscopy of $^{110}\text{Cd}$ : Evidence for weak mixing and the emergence of $\gamma$ -soft behavior

P.E. Garrett,<sup>1,2,3</sup> J. Bangay,<sup>1</sup> A. Diaz Varela,<sup>1</sup> G.C. Ball,<sup>2</sup> D.S. Cross,<sup>4</sup> G.A. Demand,<sup>1</sup> P. Finlay,<sup>1,\*</sup> A.B. Garnsworthy,<sup>2</sup> K.L. Green,<sup>1</sup> G. Hackman,<sup>2</sup> C.D. Hannant,<sup>5</sup> B. Jigmeddorj,<sup>1</sup> J. Jolie,<sup>6</sup> W.D. Kulp,<sup>7</sup> K.G. Leach,<sup>1</sup> J.N. Orce,<sup>2,8</sup> A.A. Phillips,<sup>1</sup> A.J. Radich,<sup>1,2</sup> E.T. Rand,<sup>1</sup> M.A. Schumaker,<sup>1</sup> C.E. Svensson,<sup>1</sup> C. Sumithrarachchi,<sup>1,†</sup> S. Triambak,<sup>2,‡</sup> N. Warr,<sup>5,§</sup> J. Wong,<sup>1</sup> J.L. Wood,<sup>7</sup> and S.W. Yates<sup>9</sup>

<sup>1</sup>*Department of Physics, University of Guelph, Guelph, ON, N1G2W1 Canada*

<sup>2</sup>*TRIUMF, 4004 Wesbrook Mall, Vancouver, BC, V6T2A3 Canada*

<sup>3</sup>*Excellence Cluster Universe, Boltzmannstrasse 2, D-85748, Garching, Germany*

<sup>4</sup>*Department of Chemistry, Simon Fraser University, Burnaby, BC, Canada*

<sup>5</sup>*Department of Physics & Astronomy,*

*University of Kentucky, Lexington, KY, 40506-0055 USA*

<sup>6</sup>*Institut für Kernphysik, Universität zu Köln,*

*Zùlpicherstrasse 77, D-50937 Köln, Germany*

<sup>7</sup>*Department of Physics, Georgia Institute of Technology, Atlanta, GA, USA*

<sup>8</sup>*Dept. of Physics, University of the Western Cape,*

*P/B X17, Bellville ZA-7535, South Africa*

<sup>9</sup>*Departments of Chemistry and Physics & Astronomy,*

*University of Kentucky, Lexington, KY, 40506-0055 USA*

## Abstract

A study of the  $\beta^+$ /EC decay of  $^{110}\text{In}$  into levels of  $^{110}\text{Cd}$  is combined with a reanalysis of data from a previous study of  $^{110}\text{Cd}$  with the  $(n, n'\gamma)$  reaction with monoenergetic neutrons. The  $\gamma\gamma$  coincidences from the  $^{110}\text{In}$  decay leads to many new assignments of  $\gamma$  rays observed in the  $(n, n'\gamma)$  reaction, permitting the observation of weak low-energy transitions, and setting stringent upper limits on unobserved decay branches. The uncertainties on many of the lifetimes from the  $(n, n'\gamma)$  reaction are significantly reduced, and limits are established for the lifetimes of levels too long for a direct measurement. The absence of enhanced transitions between the previously assigned phonon states and the deformed intruder states strongly suggests that mixing between the configurations is generally weak, refuting the strong-mixing scenario as an explanation of the decay pattern of the excited  $0^+$  states in  $^{110}\text{Cd}$ . The decay pattern of the non-intruder states is suggestive of a  $\gamma$ -soft rotor, or  $O(6)$  nucleus, rather than a vibrational, or  $U(5)$  pattern. The existence of a  $4p - 6h$  proton excitation in  $^{110}\text{Cd}$  is also suggested.

PACS numbers: 21.10.Re, 21.60.Ev, 23.20.Lv, 23.40.Hc

---

\* Present address: Instituut voor Kern- en Stralingsfysica, Katholieke Universiteit Leuven, B-3001, Leuven, Belgium

† Present address: National Superconducting Cyclotron Center, Michigan State University, East Lansing, MI 48824, USA

‡ Present address: Dept. of Physics and Astrophysics, University of Delhi, Delhi 110 007, India

§ Present address: Institut für Kernphysik, Universität zu Köln, Zùlpicherstrasse 77, D-50937 Köln, Germany

## I. INTRODUCTION

Historically, the Cd isotopes, especially  $^{110,112}\text{Cd}$ , have been favored examples of near-harmonic quadrupole vibrational behavior [1–3], with a two-phonon triplet of levels having  $I^\pi = 0^+, 2^+, \text{ and } 4^+$  at approximately twice the energy of the  $2_1^+$  state, and a quintuplet of levels, with  $I^\pi = 0^+, 2^+, 3^+, 4^+, \text{ and } 6^+$  at nearly  $3 \times E(2_1^+)$ . The observation of additional levels in the vicinity of the two-phonon triplet was problematic [4], however. The conclusion that these extra levels were part of a deformed coexisting structure was firmly established by Meyer and Peker [5]. These bands are based [5, 6] on  $2p - 4h$  proton “intruder” excitations across the  $Z = 50$  closed shell, and are evidenced by the enhanced  $(^3\text{He}, n)$  cross sections associated with the  $0^+$  band heads observed by Fielding *et al.* [7]. In the following sections, members of the intruder band are labeled with  $(i)$  to facilitate the discussion.

Figure 1 shows selected  $B(E2)$  values from the low-lying  $0^+$  states in  $^{110-116}\text{Cd}$ . The extremely small  $B(E2; 0_3^+ \rightarrow 2_1^+)$  values in  $^{110-114}\text{Cd}$  and the  $B(E2; 0_2^+ \rightarrow 2_1^+)$  value in  $^{116}\text{Cd}$  are noted in particular; these transitions would have  $B(E2)$  values of approximately 60 W.u. in a harmonic quadrupole vibrational picture. To explain this pattern, mixing was introduced [6, 9, 10] between the intruder states, described as having predominately an  $O(6)$  character, and vibrational states, possessing predominately  $U(5)$  character, in an interacting boson model-2 (IBM-2) formalism. Results from this calculation for  $^{110}\text{Cd}$ , using the parameters of Refs. [9, 11], are shown for selected transitions in Table I alongside calculations with no mixing between the intruder and non-intruder states and data for  $^{110,112}\text{Cd}$ . These calculations are generic for all the Cd isotopes. It is clear that the mixing is essential to explain the observed pattern.

Recent studies [11–15], using both the  $(n, n'\gamma)$  reaction and radioactive decay, have begun to characterize the higher-lying states, especially candidate states for the three-phonon multiplet in  $^{112,114,116}\text{Cd}$ . These studies have revealed consistent discrepancies between the IBM-2 model calculations, which incorporate strong mixing, and the experimental data [11, 16]. Table II shows selected higher-lying levels and transitions where the mixing has a dramatic impact on the predicted transition rate. Testing for the presence or absence of mixing requires lifetime data and precise intensities for high-lying, low-energy transitions. Lifetime data from the  $^{110}\text{Cd}(n, n'\gamma)$  have been reanalyzed – the results of which are presented below. In addition, high-statistics data for low-intensity transitions following  $\beta^+/\text{EC}$

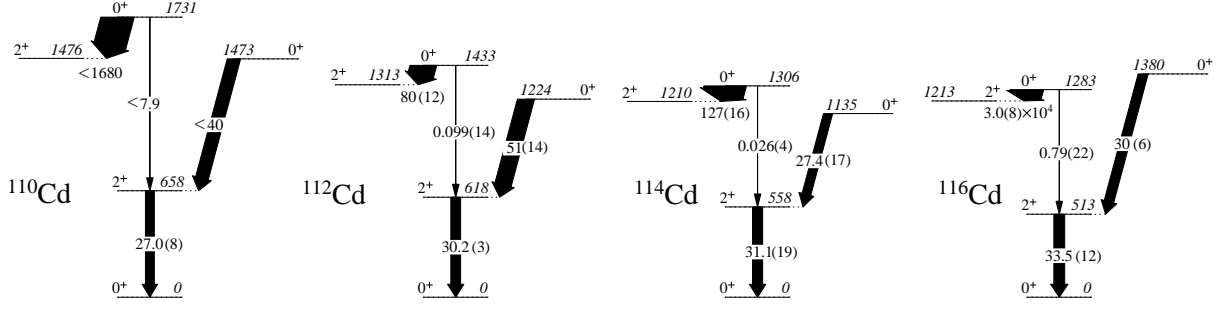


FIG. 1. Portion of the level schemes for  $^{110,112,114,116}\text{Cd}$  showing the decays from the low-lying  $0^+$  states. The observed transitions between levels are indicated by arrows with widths proportional to the  $B(E2)$  values and are labeled with the absolute  $B(E2)$  values or limits, with the uncertainties in parentheses. Data are taken from Ref. [8] and the present results for  $^{110}\text{Cd}$ .

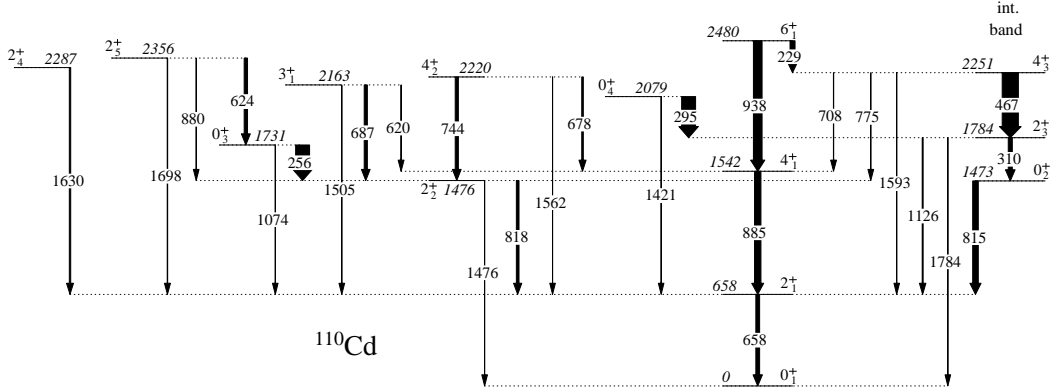


FIG. 2. Portion of the low-lying level scheme for  $^{110}\text{Cd}$ . The observed transitions between levels are indicated by arrows with widths proportional to  $B(E2)$  values. The levels on the right side of the figure are assigned as members of the deformed intruder band based on a  $2p - 4h$  proton excitation [5, 6, 23, 24]. The 1731-, 1475-, and 1542-keV levels were previously assigned as the  $0^+$ ,  $2^+$ , and  $4^+$  two-phonon triplet, and the 2079-keV ( $0_4^+$ ), 2356-keV ( $2_5^+$ ), 2163-keV ( $3_1^+$ ), 2220-keV ( $4_2^+$ ), and 2480-keV ( $6_1^+$ ) levels as members of the three-phonon quintuplet [3, 18, 19, 23, 25].

decay of  $^{110}\text{In}$  have been obtained. The experimental procedure which provides the transition intensities is described below.

TABLE I. Transition rates, in W.u., from IBM-2 calculations for  $^{110}\text{Cd}$ , incorporating mixing between the intruder and non-intruder states and without mixing of the configurations, compared with the experimental results for both  $^{110}\text{Cd}$  and  $^{112}\text{Cd}$  [8].

Transition	IBM-2		Experimental	
	mixed	unmixed	$^{110}\text{Cd}$	$^{112}\text{Cd}$
$2_1^+ \rightarrow 0_1^+$	27	26	27.0(8)	30.2(3)
$0_2^+(i) \rightarrow 2_1^+$	31	0	< 40	51(14)
$0_3^+ \rightarrow 2_2^+$	55	7.6	< 1680	80(12)
$0_3^+ \rightarrow 2_1^+$	1.1	24	< 7.9	0.0099(14)

## II. EXPERIMENTAL DETAILS AND RESULTS

The  $^{110}\text{In}$  decay experiment was performed with the  $8\pi$   $\gamma$ -ray spectrometer [17] at the TRIUMF-ISAC facility. A  $65\text{-}\mu\text{A}$ , 500-MeV proton beam was directed onto a  $^{nat}\text{Ta}$  target. Products that diffused to the surface of target foils were ionized with a Re surface-ion source and passed through a magnetic mass separator set to select singly charged  $A = 110$  ions. The resultant beam delivered to the experimental area consisted of  $1.2 \times 10^7 \text{ s}^{-1}$  of the  $I^\pi = 7^+$   $t_{1/2} = 4.9 \text{ hr}$   $^{110}\text{In}^g$  and  $1.7 \times 10^6 \text{ s}^{-1}$  of the  $I^\pi = 2^+$   $t_{1/2} = 1.15 \text{ hr}$   $^{110}\text{In}^m$ . The beam was deposited onto a FeO coated mylar tape at the center of the  $8\pi$  spectrometer which consisted of 20 high-purity Ge (HPGe) detectors with bismuth germanate (BGO) Compton-suppression shields. The average source-to-Ge-detector distance was 14 cm. A BC-422Q fast plastic scintillator with a solid angle of approximately 20% was located immediately behind the beam deposition point, while the 5 Si(Li) detectors of the PACES array for conversion-electron studies were positioned upstream. The data were collected in scaled-down  $\gamma$ -singles,  $\gamma\gamma$ , and  $\gamma e^-$  coincidences during the approximately 1 h of beam deposition plus 1 h of decay, after which the source position on the tape was moved to a point outside the array behind a lead wall and the cycle repeated.

The details of the  $(n, n'\gamma)$  experiment have been presented in Refs. [18, 19]. In the reanalysis of the data, the spectra were fitted with a focus on low-intensity transitions and the consistency of fits across spectra. This procedure resulted in the assignment [20] of over 170  $\gamma$  rays to  $^{110}\text{Cd}$ , with nearly all placed, compared to 128 identified in the earlier analysis

TABLE II. Selected transition rates, in W.u., from IBM-2 calculations with and without mixing of the intruder and non-intruder states, which show the sensitivity to mixing. The subscript on the level indicates the experimental ordering of the levels, not necessarily that of the calculation.

Transition	IBM-2	
	mixed	unmixed
$2_3^+(i) \rightarrow 4_1^+$	12	0
$2_3^+(i) \rightarrow 2_2^+$	10	0
$0_4^+ \rightarrow 2_3^+(i)$	33	0
$0_4^+ \rightarrow 2_2^+$	18	33
$4_2^+ \rightarrow 2_3^+(i)$	44	0
$2_5^+ \rightarrow 2_3^+(i)$	23	0
$6_1^+ \rightarrow 4_3^+(i)$	6.6	0

with 77 placed in the level scheme. This high level of placement success could not have been achieved without access to the new  $^{110}\text{In}$  decay data.

The  $\gamma$ -ray branching fractions were determined from both the  $(n, n'\gamma)$  data and the  $^{110}\text{In}$  decay data. The  $(n, n'\gamma)$  data were based on  $\gamma$ -ray singles measurements only, whereas the  $^{110}\text{In}$  decay data used  $\gamma$ -ray coincidence gating, with gates taken from above or below. When gating from above, the standard method was used where the intensity of the  $\gamma$  ray of interest was divided by the total intensity out of that level. Gating from below required the method described in Ref. [21] utilizing

$$N_{12} = \mathcal{N} I_{\gamma_1} \epsilon(\gamma_1) B_{\gamma_2} \epsilon(\gamma_2) \epsilon_C \eta(\theta_{12}) \quad (1)$$

with  $N_{12}$  the number of counts in the coincidence peak between two cascading  $\gamma$  rays,  $I_{\gamma_1}$  is the intensity of the “feeding”  $\gamma$  ray of the pair,  $B_{\gamma_2}$  is the branching fraction of the “draining” transition  $\gamma_2$ , and  $\epsilon(\gamma)$  the detection efficiency at energy  $E_\gamma$ . The factor  $\mathcal{N}$  is an overall normalization constant that characterizes a given decay data set,  $\epsilon_C$  reflects the change in the detection efficiency due to the coincidence condition, and  $\eta(\theta_{12})$  is the effect of the angular correlation. For the present data, the assumption is made that the time conditions applied during the sorting of the data did not distort the detection efficiency, and corrections due to angular correlations and summing effects are in general below  $\pm 3\%$  due to the excellent symmetry of the  $8\pi$  spectrometer resulting from the icosahedral positioning

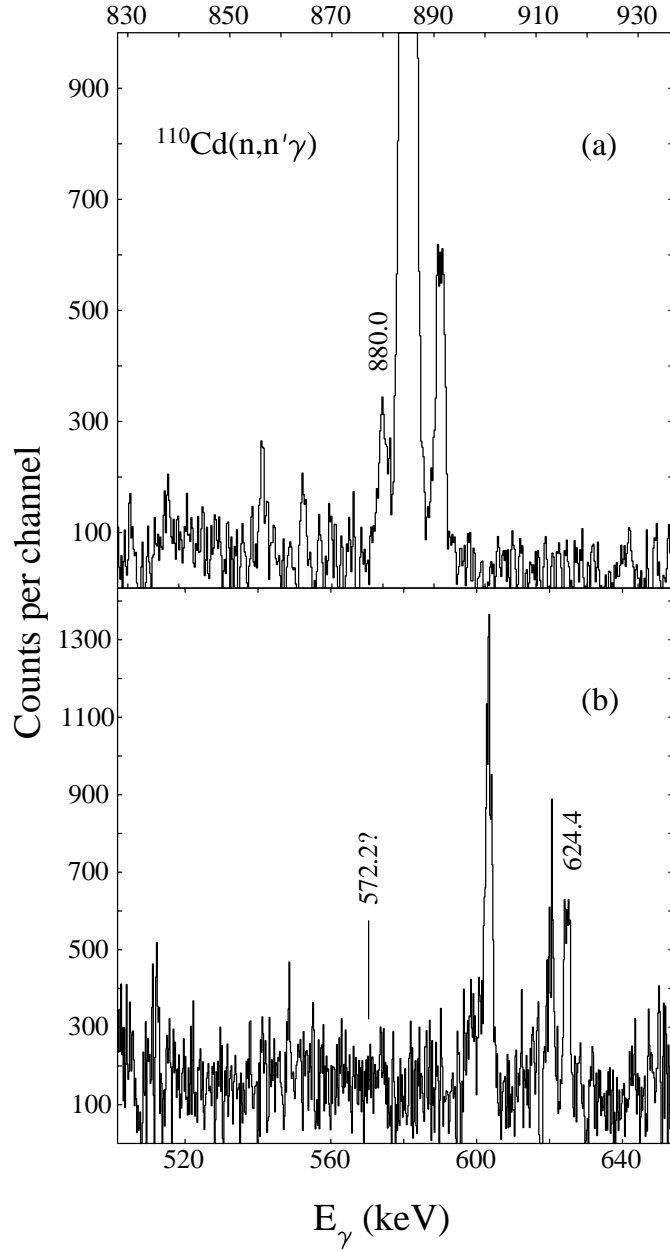


FIG. 3. Portions of the  $\gamma$ -ray spectrum obtained by summing the excitation function spectra obtained with the  $(n, n'\gamma)$  reaction for neutron energies from 2.5 to 2.8 MeV and subtracting a 2.4-MeV spectrum normalized to the total number of neutrons for the 2.5–2.8 MeV data. The peaks of interest are labeled by their energies in keV. The top panel (a) displays the region around the newly placed 880-keV  $2_5^+ \rightarrow 2_2^+$   $\gamma$  ray, whereas the bottom panel (b) displays the 624-keV  $2_5^+ \rightarrow 0_3^+$   $\gamma$  ray, and the position of a hypothetical peak corresponding to a 572-keV  $2_5^+ \rightarrow 2_3^+(i)$  transition.

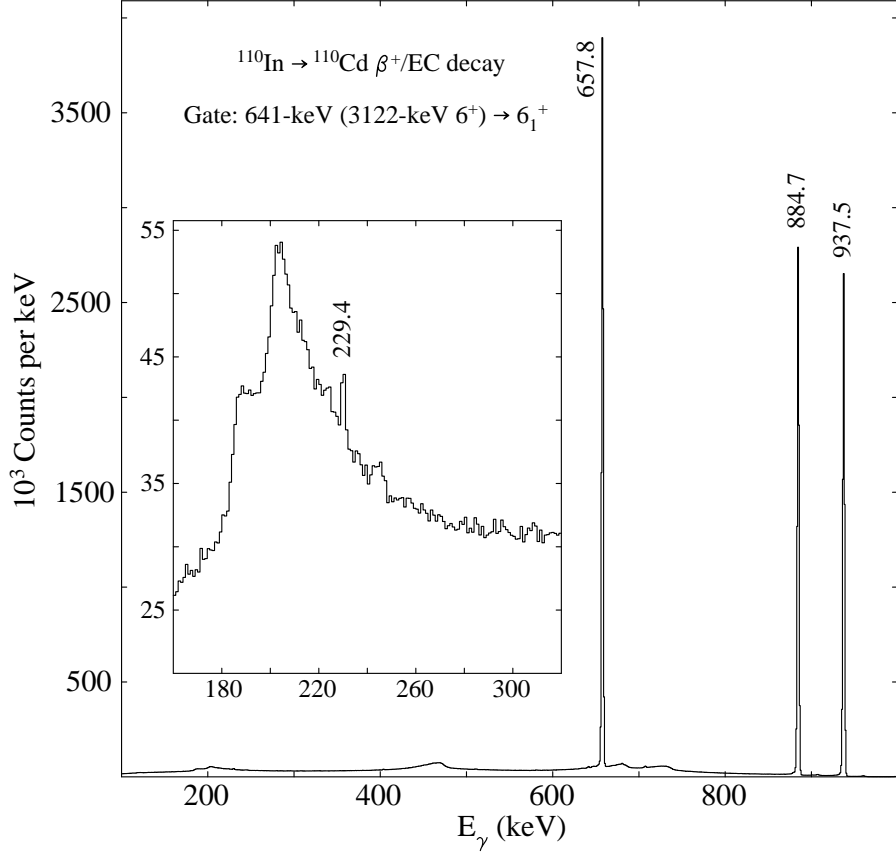


FIG. 4. Portion of the  $\gamma$ -ray coincidence spectrum from the  $^{110}\text{In}$  decay obtained by placing a gate on the 641-keV  $\gamma$  ray that feeds the 2480-keV  $6_1^+$  state. The peaks are labeled by their energies in keV. The inset shows the expanded region near the 229-keV  $6_1^+ \rightarrow 4_3^+(i)$   $\gamma$  ray that leads to its firm assignment with a branching fraction of  $5.1(3) \times 10^{-4}$ .

of the  $\gamma$ -ray detectors. Relabeling  $I'_{\gamma_1} = N_{12}/\epsilon(\gamma_1)$ , the branching ratio for any level can be found from

$$BR(\gamma_1) = \frac{I'_{\gamma_1}}{B_{\gamma_2} \epsilon(\gamma_2)} \quad (2)$$

$$\sum_j \frac{I'_{\gamma_{1j}}}{B_{\gamma_{2j}} \epsilon(\gamma_{2j})}$$

where the summation over  $j$  extends to all transitions decaying from the level of interest. When there was no indication of a peak present, a limit was calculated using the procedure outlined in Ref. [22]. When there was weak evidence of a peak in the region of interest, the branching ratio was determined as if a real peak was present and the upper limit calculated by adding  $2\sigma$  to the central branching ratio value.

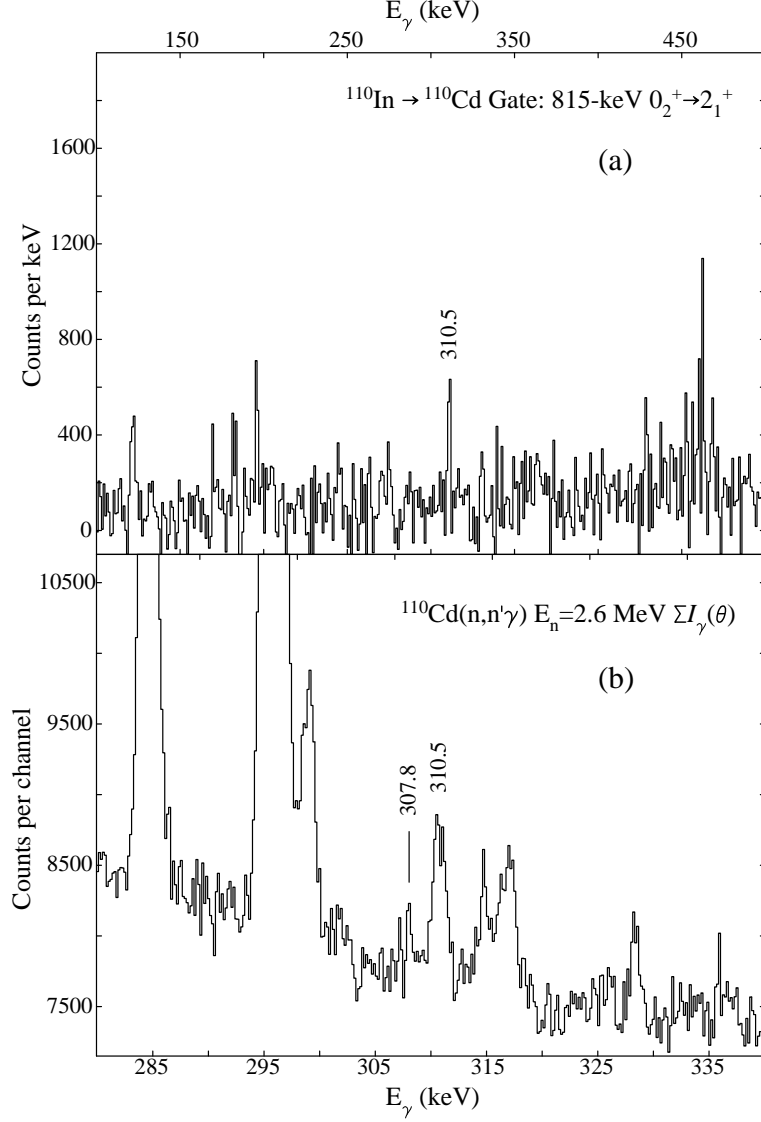


FIG. 5. (a) Portion of the spectrum of  $\gamma$  rays in coincidence with the 815-keV  $0_2^+(i) \rightarrow 2_1^+$   $\gamma$  ray, and the angular distribution data from the  $(n, n'\gamma)$  reaction at  $E_n = 2.6$  MeV. The top panel displays the coincidence of the 310.5-keV  $2_3^+(i) \rightarrow 0_2^+(i)$   $\gamma$  ray, leading to a measured branching fraction of  $0.0037 \pm 0.0004$ , confirming the 1783-keV level as the  $2^+$  rotational band member of the deformed intruder band based on the 1473-keV  $0_2^+(i)$  state. (b) Singles spectrum was obtained by the summation of spectra taken at 12 angles from  $30^\circ$  to  $152^\circ$ . The 310.5-keV  $\gamma$  ray is clearly visible, with only weak evidence of a peak at the location of a 307.8-keV  $\gamma$  ray. This location corresponds to that of a transition from the 1783-keV level feeding the 1475-keV  $2_2^+$  level; an upper limit for the branching fraction of  $< 9 \times 10^{-4}$  is established.

The low-lying level scheme of  $^{110}\text{Cd}$  is shown in Fig. 2. The present work has led to the new placement of a transition amongst the levels shown in Fig. 2, the 880-keV  $\gamma$  ray from the 2356-keV  $2_5^+$  state, and has firmly established the 229-keV  $\gamma$  ray from the 2480-keV  $6_1^+$  state. Figure 3 displays portions of the spectrum obtained by summing spectra from the  $(n, n'\gamma)$  excitation functions from 2.5 to 2.8 MeV, and subtracting a normalized 2.4-MeV spectrum. The resulting spectrum highlights transitions from levels with thresholds between 2.2 MeV and 2.7 MeV, while largely removing the peaks from  $\gamma$  rays with thresholds below 2 MeV. In the top portion of Fig. 3, panel a), the newly assigned 880-keV  $\gamma$  ray is clearly visible. The 572-keV  $\gamma$  ray from the  $2_5^+$  state feeding the  $2_3^+(i)$  intruder state remains unobserved, as shown in panel b) of Fig. 3. Figure 4 displays a portion of the spectrum from the  $^{110}\text{In}$  decay in which a gate has been placed on a 641-keV  $\gamma$  ray feeding the 2480-keV  $6_1^+$  level. The inset shows the evidence for the firm placement of the 229-keV  $6_1^+ \rightarrow 2251\text{-keV } 4_3^+(i)$   $\gamma$  ray. The extracted branching fraction is  $5.1(3) \times 10^{-4}$ . In addition to these new  $\gamma$  rays, the branching fractions have been refined considerably for many of the remaining transitions. For example, the 310.5-keV  $\gamma$  ray corresponding to the  $2_3^+ \rightarrow 0_2^+(i)$  transition in the intruder band was previously reported to have branching fractions of 0.15% (no uncertainty given) [5], and  $0.003 \pm 0.001$  [18]. Using coincidence gating in the  $^{110}\text{In}$  decay data, as shown in the panel a) of Fig. 5, the present result is  $0.0037 \pm 0.0004$ . In panel b) of Fig. 5, the  $(n, n'\gamma)$  angular distribution data, taken with  $E_n = 2.6$  MeV, have been summed to provide increased sensitivity for low-energy transitions. The 310.5-keV  $\gamma$  ray is clearly visible. At the location corresponding to the  $2_3^+(i) \rightarrow 2_2^+$  transition, 307.8 keV, there is an excess of counts, but no firm identification of a peak can be made; a fit to the region yields an upper limit for the branching fraction of  $< 9 \times 10^{-4}$ , and thus a limit for the  $B(E2; 2_3^+(i) \rightarrow 2_2^+)$  transition of  $< 8$  W.u.

TABLE III: Selected results for levels in  $^{110}\text{Cd}$  from the  $(n, n'\gamma)$  reaction and  $\beta^+$ /EC decay of  $^{110}\text{In}$ . Uncertainties are listed in parentheses. The  $\gamma$ -ray energy uncertainties are statistical only, and do not include an estimated 20 eV systematic uncertainty. The  $I_\gamma$  values are the relative intensity of the observed  $\gamma$  rays for each level, normalized to 1.0, derived from the  $^{110}\text{In}$  decay unless otherwise noted. For some transitions, the angular distribution analysis leads to ambiguities in the value of the mixing ratio  $\delta$  [from the reanalysis of the  $(n, n'\gamma)$  data]; the second value listed has the larger  $\chi^2$  value, but cannot be excluded. The final column lists the deduced absolute  $B(E2)$  value in W.u., except for those contained in square brackets, which are relative values.

$E_i$ (keV)	$I_i^\pi$	$E_\gamma$ (keV)	$E_f$ (keV)	$I_f^\pi$	$I_\gamma$	$\delta$	$\tau$ (fs)	$B(E2; I_i \rightarrow I_f)$ (W.u.)
657.765(2) <sup>a</sup>	$2_1^+$	657.760(1) <sup>a</sup>	0.0	$0_1^+$	1.0			27.1(8) <sup>a</sup>
1473.090(6)	$0_2^+(i)$	815.323(3)	657.8	$2_1^+$	1.0		> 1800	< 40
1475.801(5)	$2_2^+$	818.323(3)	657.8	$2_1^+$	0.643(10)	$-2.17^{+0.35}_{-0.36}$	$1950^{+500}_{-330}$	19(4)
		1475.799(8)	0.0	$0_1^+$	0.357(10)			0.68(14)
1542.458(5)	$4_1^+$	884.688(3)	657.8	$2_1^+$	1.0			42(7) <sup>a</sup>
1731.312(9)	$0_3^+$	255.547(15)	1475.8	$2_2^+$	0.143(8)		> 2000	< 1680
		1073.549(7)	657.8	$2_1^+$	0.857(8) <sup>b</sup>			< 7.9
1783.561(7)	$2_3^+(i)$	307.8 <sup>b</sup>	1475.8	$2_2^+$	< 0.0009 <sup>c</sup>		$1160^{+170}_{-140}$	< 8
		310.515(38)	1473.1	$0_2^+(i)$	0.0037(4)			29(5)
		1125.789(5)	657.8	$2_1^+$	0.772(8)	$0.186^{+0.038}_{-0.028}$		$0.32^{+0.10}_{-0.14}$
						$1.52^{+0.12}_{-0.09}$		$6.7^{+1.0}_{-0.9}$
		1783.583(14)	0.0	$0_1^+$	0.224(6)			0.28(4)
2078.885(22) <sup>a</sup>	$0_4^+$	295.3	1783.6	$2_3^+(i)$	0.791(21)			[100]
		603.1 <sup>b</sup>	1475.8	$2_2^+$	< 0.18			[< 0.65]
		1421.1 <sup>b</sup>	657.8	$2_1^+$	0.209(21)			[0.010]
2162.809(7)	$3_1^+$	379.2 <sup>b</sup>	1783.6	$2_3^+(i)$	< 0.003 <sup>b</sup>		$1640^{+700}_{-380}$	< 5
		620.300(20)	1542.5	$4_1^+$	0.117(4)	$-0.36^{+0.04}_{-0.05}$		$2.4^{+0.9}_{-0.8}$
						$-1.93^{+0.24}_{-0.28}$		39(12)
		687.004(4)	1475.8	$2_2^+$	0.287(9)	$-1.79(10)$		22.7(69)
		1505.046(11)	657.8	$2_1^+$	0.596(10)	$-1.47^{+0.10}_{-0.11}$		0.85(25)
2220.087(7)	$4_2^+$	436.5 <sup>b</sup>	1783.6	$2_3^+(i)$	< 0.0003		$1510^{+1140}_{-460}$	< 0.5
		677.623(4)	1542.5	$4_1^+$	0.630(9)	$-0.41(3)$		$10.7^{+4.9}_{-4.8}$
		744.307(10)	1475.8	$2_2^+$	0.293(9)			22(10)
		1562.324(52)	657.8	$2_1^+$	0.076(3)			0.14(6)
2250.580(8)	$4_3^+(i)$	466.997(16)	1783.6	$2_3^+(i)$	0.104(4)		$1080^{+450}_{-250}$	115(35)
		708.122(4)	1542.5	$4_1^+$	0.813(6)	$0.131^{+0.044}_{-0.036}$		$1.8^{+1.0}_{-1.5}$
		774.91(12)	1475.8	$2_2^+$	0.0160(7)			1.2(4)
		1592.824(58)	657.8	$2_1^+$	0.067(3)			0.14(4)

Continued on next page

TABLE III (continued)

$E_i$ (keV)	$I_i^\pi$	$E_\gamma$ (keV)	$E_f$ (keV)	$I_f^\pi$	$I_\gamma$	$\delta$	$\tau$ (fs)	$B(E2; I_i \rightarrow I_f)$ (W.u.)
2355.776(17)	$2_5^+$	572.2 <sup>b</sup>	1783.6	$2_3^+(i)$	$< 0.006^c$		$484_{-38}^{+47}$	$< 5$
		624.364(36)	1731.3	$0_3^+$	0.0416(11) <sup>c</sup>			24.2(22)
		813.3 <sup>b</sup>	1542.5	$4_1^+$	$< 0.03$			$< 5$
		880.0 <sup>b</sup>	1475.1	$2_2^+$	0.0217(13) <sup>c</sup>	$0.66_{-0.34}^{+0.51}$		$0.7_{-0.6}^{+0.5}$
		882.7 <sup>b</sup>	1473.1	$0_2^+(i)$	$< 0.017$			$< 1.9$
2479.971(74)	$6_1^+$	1698.029(12)	657.8	$2_1^+$	0.9367(16) <sup>c</sup>	$2.7(3)$	$d$	3.2(3)
		229.4 <sup>b</sup>	2250.6	$4_3^+(i)$	0.00051(3)	$-0.050_{-0.045}^{+0.034}$		$0.009_{-0.008}^{+0.023}$
		259.9 <sup>b</sup>	2220.1	$4_2^+$	$< 0.0001$			$< 5$
		937.511(44)	1542.5	$4_1^+$	0.99949(3)			62(18)

<sup>a</sup>Value taken from Ref. [26].

<sup>b</sup>Value obtained from difference in level energies.

<sup>c</sup>Branching fraction from  $(n, n'\gamma)$  data.

<sup>d</sup>Lifetime taken from Ref. [27].

Table III presents the results from the present work. Combining the new lifetime values with the branching ratios, together with their limits, leads to the  $B(E2)$  values listed. The lifetimes are, in general, in excellent agreement with those of the previous analysis [18], but the uncertainties have been reduced considerably due to more precise fitting of the spectra. An exception is the lifetime of the 2220-keV  $4^+$  level with  $\tau = 1510_{-460}^{+1140}$  fs from the present analysis compared with  $970_{-230}^{+430}$  fs [18, 19].

### III. DISCUSSION AND INTERPRETATION

The new results confirm many of the previous conclusions regarding the structure of  $^{110}\text{Cd}$ , and more generally, of  $^{110-116}\text{Cd}$ . The structural details that are confirmed are first discussed, followed by the new insights provided by the present study.

#### A. Intruding $\pi 2p - 4h$ configuration

The intruder band is well established, with the  $0_2^+(i)$  state as the band head, a 1784-keV  $2^+$  member, a 2251-keV  $4^+$  member, and a 2877-keV  $6^+$  member [5, 7, 23, 24]. The improved branching fraction for the  $2_3^+(i) \rightarrow 0_2^+(i)$  transition from the coincidence gating and the new lifetime result yields  $B(E2; 2_3^+(i) \rightarrow 0_2^+(i)) = 29 \pm 5$  W.u. which can be compared with  $47_{-7}^{+10}$ ,  $65 \pm 9$ , and  $86_{-30}^{+24}$  W.u., respectively, for the corresponding transitions in  $^{112,114,116}\text{Cd}$

[11]. There is thus a definite trend of increasing collectivity in the deformed intruder band with increasing neutron number.

The  $0_2^+(i)$  level is assigned as the head of the deformed intruder band based on the strong  $2_3^+(i) \rightarrow 0_2^+(i)$  transition ( $29 \pm 5$  W.u.) and also the strong population in the ( ${}^3\text{He}, n$ ) two-proton transfer reaction [7]. Unfortunately, the lifetime of the  $0_2^+(i)$  state is too long to be measured in the present work, and a lower limit of 1800 fs is determined, establishing a  $B(E2)$  upper limit of 40 W.u. for its decay to the  $2_1^+$  level. The  $0_4^+$  level, at 2079-keV, has a strongly favored decay to the  $2^+$  member of the intruder band at 1784 keV (the  $2_3^+(i)$  level). Figure 6 displays a portion of the  $\gamma$ -ray spectrum of coincidences with a 1397-keV  $\gamma$  ray from the 3475-keV  $I = 1 \rightarrow 2079$ -keV  $0_4^+$  level, clearly showing the dominance of the 295-keV  $0_4^+ \rightarrow 2_3^+(i)$   $\gamma$  ray. Also noted is the location of a potential 603-keV  $0_4^+ \rightarrow 2_2^+$  transition; the extracted upper limit for the branch is  $< 0.18$ . In Refs. [11, 28] it was argued that the  $0_4^+$  states in the  ${}^{110,112,114,116}\text{Cd}$  were excitations built on the intruder band, based on their “V”-shaped pattern of excitation energies, with a minimum near the mid-shell, similar to the lowest  $0^+$  intruder state, and their preferred  $\gamma$  decay to the first  $2^+$  state of the intruder band.

## B. Previous Vibrational Interpretation

The  $B(E2; 2_1^+ \rightarrow 0_1^+)$  value of 27.0(8) W.u. is clearly enhanced and has a magnitude expected for a quadrupole phonon excitation. At approximately twice the energy of the 658-keV one-phonon state, there should exist a triplet of levels, with spin-parities  $0^+$ ,  $2^+$ , and  $4^+$  and  $B(E2)$  values equal to twice that for decay to the one-phonon level, i.e., 55 W.u. The  $B(E2; 4_1^+ \rightarrow 2_1^+)$  value of  $42 \pm 7$  W.u. is in reasonable agreement with this expectation. The  $2_2^+$  level at 1476 keV, however, has  $B(E2; 2_2^+ \rightarrow 2_1^+) = 19 \pm 4$  W.u., nearly a factor of 3 smaller than expected. The  $0_3^+$  level at 1731 keV has a lifetime too long to be determined by the Doppler shift method, but has a strongly preferred decay to the  $2_2^+$  level at 1476 keV. Thus, the only  $0^+$  level that may have an enhanced  $B(E2)$  value to the  $2_1^+$  level, the one-phonon state, is the intruder band head.

The small magnitude of the  $B(E2; 2_2^+ \rightarrow 2_1^+)$  value and the fact that the only possible enhanced  $B(E2; 0^+ \rightarrow 2_1^+)$  value is from the deformed-intruder band head casts doubt on the appropriateness of the vibrational model for  ${}^{110}\text{Cd}$ . As shown in Table I, this decay

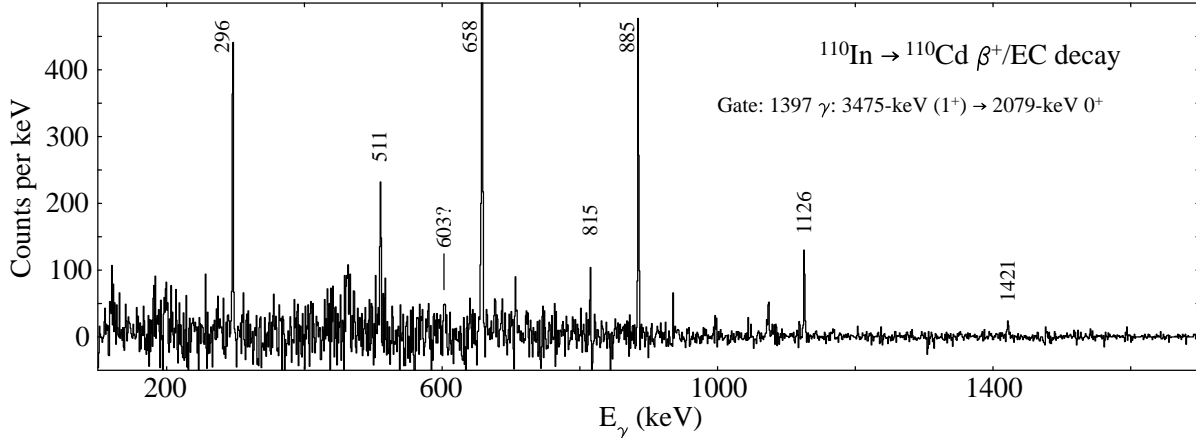


FIG. 6. Portion of the  $\gamma$ -ray spectrum in coincidence with the 1397-keV  $\gamma$  ray decaying from a  $I = 1$  level at 3475 keV to the 2079-keV  $0_4^+$  level. The  $\gamma$  rays are labeled by their energies in keV. Of note are the relative intensities of the 295 and 1421-keV  $\gamma$  rays. The position of a hypothetical 603-keV  $0_4^+ \rightarrow 2_2^+$   $\gamma$  ray is indicated.

pattern could be explained within the interacting boson model (IBM) by incorporating strong mixing between the vibrational phonons and deformed intruder states. To explain the near vanishing of the  $B(E2; 0_3^+ \rightarrow 2_1^+)$  and the enhancement of the  $B(E2; 0_2^+(i) \rightarrow 2_1^+)$ , nearly maximal mixing between the phonon and intruder configurations was invoked that resulted in destructive interference for  $0_3^+ \rightarrow 2_1^+$  decay, and constructive interference for the  $0_2^+(i) \rightarrow 2_1^+$  decay [6, 9].

With the more precise lifetimes and upper limits on transitions determined in the present study, a detailed comparison with the IBM-2 calculations, assuming predominately vibrational character for the non-intruder states, can now be made and is shown in Table IV. First, it should be noted that many of the  $B(E2)$  values are very small and do not provide a means of distinguishing between the mixed and unmixed calculations. The strong-mixing calculations appear to reproduce the decay pattern for the intruder band, the two-phonon triplet, and the  $3^+$  member of the three-phonon quintuplet. However, the calculations were carefully tuned to reproduce the decay of the  $0_2^+(i)$  and  $0_3^+$  levels by adjusting the mixing matrix element and the parameter  $\Delta$  that describes the position of the intruder configuration with respect to the normal configuration. The  $2_2^+$ ,  $2_3^+(i)$ , and  $3_1^+$  levels all have *weak* mixing with nearby levels. This can be understood as due to the common  $O(5)$  subgroup

TABLE IV. Selected  $E2$  transition rates, in W.u., from IBM-2 calculations, with and without mixing the intruder and non-intruder states, compared to the experimental results for  $^{110}\text{Cd}$ . Quantities in square brackets are relative  $B(E2)$  values. Transitions with two possible solutions for the  $E2/M1$  mixing ratio  $\delta$  have the  $B(E2)$  value for the most favored  $\delta$  listed first.

Transition	$B(E2; I_i^{\pi} \rightarrow I_f^{\pi})$		
	mixed	unmixed	Experimental
$2_1^+ \rightarrow 0_1^+$	27	26	27.0(8)
$0_2^+(i) \rightarrow 2_1^+$	31	0	< 40
$2_2^+ \rightarrow 0_1^+$	0.2	0.19	0.68(14)
$2_2^+ \rightarrow 2_1^+$	36	31	19(4)
$4_1^+ \rightarrow 2_1^+$	43	39	42(7)
$0_3^+ \rightarrow 2_2^+$	55	7.6	< 1680
$0_3^+ \rightarrow 2_1^+$	1.1	24	< 7.9
$2_3^+(i) \rightarrow 4_1^+$	12	0	
$2_3^+(i) \rightarrow 0_2^+(i)$	59	128	29(5)
$2_3^+(i) \rightarrow 2_2^+$	10	0	< 8
$2_3^+(i) \rightarrow 2_1^+$	0.0049	0	$0.32_{-0.14}^{+0.10}, 6.7_{-0.9}^{+1.0}$
$0_4^+ \rightarrow 2_3^+(i)$	33	0	[100]
$0_4^+ \rightarrow 2_2^+$	18	33	[< 0.65]
$0_4^+ \rightarrow 2_1^+$		0.29	[0.010]
$3_1^+ \rightarrow 4_1^+$	13	11	$2.4_{-0.8}^{+0.9}, 39(12)$
$3_1^+ \rightarrow 2_2^+$	37	34	22.7(69)
$3_1^+ \rightarrow 2_3^+(i)$	0.43	0	< 5
$3_1^+ \rightarrow 2_1^+$	0.22	0.25	0.85(25)
$4_2^+ \rightarrow 2_3^+(i)$	44	0	< 0.5
$4_2^+ \rightarrow 4_1^+$	22	17	$10.7_{-4.8}^{+4.9}$
$4_2^+ \rightarrow 2_2^+$	35	22	22(10)
$4_2^+ \rightarrow 2_1^+$	0.20	0.035	0.14(6)
$4_3^+(i) \rightarrow 2_3^+(i)$	107	182	115(35)
$4_3^+(i) \rightarrow 4_1^+$	1.2	0	$1.8_{-1.5}^{+1.0}$
$4_3^+(i) \rightarrow 2_2^+$	0.066	0	1.2(4)
$4_3^+(i) \rightarrow 2_1^+$	0.22	0	0.14(4)
$2_5^+ \rightarrow 0_3^+$	16	13	24.2(22)
$2_5^+ \rightarrow 4_1^+$	4.5	8.6	< 5
$2_5^+ \rightarrow 2_2^+$	0.83	3.6	$0.7_{-0.6}^{+0.6}$
$2_5^+ \rightarrow 0_2^+(i)$	0.87	0	< 1.9
$2_5^+ \rightarrow 2_3^+(i)$	23	0	< 5
$2_5^+ \rightarrow 2_1^+$	0.033	0.0011	$3.2(3), 0.009_{-0.008}^{+0.023}$
$2_5^+ \rightarrow 0_1^+$	0.28	0.15	
$6_1^+ \rightarrow 4_3^+(i)$	6.6	0	36(11)
$6_1^+ \rightarrow 4_2^+$	2.6	0.06	< 5
$6_1^+ \rightarrow 4_1^+$	54	46	62(18)

in both configurations [29]. The calculated wave functions for the  $2_2^+$  and  $2_3^+(i)$  levels have amplitudes of  $0.94|2_2^n\rangle$  and  $0.91|2_1^i\rangle$ , where the superscripts  $n$  and  $i$  refer to the unmixed “normal” phonon and the intruder configurations, respectively. While the mixing of the  $2_2^+$  and  $2_3^+(i)$  levels is small, it still gives rise to an enhancement of the  $2_3^+(i) \rightarrow 2_2^+$  transition, with a calculated  $B(E2)$  value of 10 W.u.; the experimental upper limit is  $< 8$  W.u., implying that the mixing is even less than calculated. The  $3_1^+$  level has  $0.96|3_1^n\rangle$  as the dominating component in its wave function. Only the  $4_3^+(i)$  level, a member of the intruder band, has a significant mixing of its wave function with dominating components  $0.64|4_2^n\rangle + 0.74|4_1^i\rangle$ . While it might be expected that there should be a strong  $4_3^+(i) \rightarrow 2_2^+$  transition based on the composition of the wave function in the calculations, the transition is suppressed in precisely the same manner as the  $0_3^+ \rightarrow 2_1^+$  transition.

Turning to the remaining levels that display enhanced transitions to the lower-lying states, a different picture emerges. The  $0_4^+$  level at 2079 keV, previously suggested as a member of the three-phonon quintuplet [3, 18, 19, 23, 25], has a dominant decay to the  $2^+$  member of the intruder band. While the  $0_4^+$  level in the calculations possesses an enhanced decay to the  $2^+$  intruder band member, an enhanced decay is also predicted to the  $2^+$  two-phonon level. Experimentally, the  $B(E2)$  value of this latter decay is a factor of at least 150 smaller (note that only an upper limit on the decay branch exists) than the  $B(E2)$  value for decay to the intruder band. The  $4_2^+$  level has enhanced decays to both the  $2_2^+$  and  $4_1^+$  levels, as would be expected for a three-phonon state, but is also predicted to have its strongest  $B(E2)$  value (44 W.u.) for decay to the  $2_3^+(i)$  intruder state – a result of the mixing between the  $4_2^n$  and  $4_1^i$  states. The experimental upper limit is  $< 0.5$  W.u. The  $2_5^+$  level is predicted to have an enhanced decay to the  $2_3^+(i)$  intruder band member of 23 W.u., whereas experimentally an upper limit of  $< 5$  W.u. is established.

The remarkable feature now illuminated is the apparent *absence* of mixing of the intruder with non-intruder configurations, except perhaps for the ground-state band. The only level with firmly established large  $B(E2)$  values to both the normal and intruder states is the  $6_1^+$  member of the ground state band that decays to the  $4_3^+(i)$  member of the intruder band with  $36 \pm 11$  W.u. Based on systematics [11], it is also likely that the intruder band head has a large  $B(E2)$  value for decay to the  $2_1^+$  level just below the limit of 40 W.u. established here. Further evidence for the weak mixing between the ground-state and intruder bands is from the weakly enhanced  $\rho^2(E0)$  values between the lower-spin band members [16, 30].

No other level is known to exhibit enhanced  $E2$  decays to both configurations <sup>1</sup>. In the strong-mixing scenario required to explain the decays of the  $0_2^+(i)$  and  $0_3^+$  levels, a natural consequence is the mixing of other excited states, leading to enhanced  $E2$  decays between the configurations.

Rejecting the vibrational-intruder strong-mixing scenario has the immediate consequence that the decays of the excited  $0_2^+(i)$  and  $0_3^+$  levels are no longer explained, as illustrated in Table I. However, Table IV shows that the predicted transition strengths from other levels with large  $B(E2)$  values are either relatively unchanged, or in *better* agreement, in the calculation without mixing. For example, the predicted decay of the  $4_2^+$  level to the intruder  $2_3^+(i)$  band member is in much better agreement with the experimental data in the unmixed calculation, and similarly for the  $2_5^+$  level. Overall, the result of the non-mixing calculation is judged to be no better, nor worse, than that of the mixed calculation (note that the effective charges for the intruder configuration have not been adjusted, but could be so as to reproduce the intruder  $B(E2; 2_3^+(i) \rightarrow 0_2^+(i))$  value which would renormalize the  $B(E2; 4_3^+(i) \rightarrow 2_3^+(i))$  value as well). The disagreement with experimental data stems largely from the fact that the underlying configuration for the normal states was taken as vibrational, i.e., dominated by that expected for  $U(5)$  symmetry.

### C. Alternative Interpretations

If the underlying non-intruder configuration is not vibrational, the question arises as to what it may be. A key would seem to be the near vanishing of the  $B(E2; 0_3^+ \rightarrow 2_1^+)$  value, while at the same time an enhancement of the  $B(E2; 0_3^+ \rightarrow 2_2^+)$  value is exhibited. This behavior is that expected for  $O(6)$  nuclei, or the  $\gamma$ -soft picture of Wilets and Jean [31]. Further, the rearrangement of the levels into band structures, as shown, for example, in Fig. 7 of Ref. [16] results in a  $K = 2$  band staggering which also is in accord with that expected for a  $\gamma$ -soft nucleus.

Several experimental observations remain problematic in such an interpretation. Foremost, there is no explanation for the enhanced intruder  $B(E2; 0_2^+(i) \rightarrow 2_1^+)$  value, which arose from strong mixing in the previous scenario. Further, the Wilets-Jean model, or the

---

<sup>1</sup> This statement includes not only the levels discussed here, but also all other excited states below 3 MeV in excitation energy, the results of which will be published separately [20].

$O(6)$  limit of the IBM, predicts identically zero for the quadrupole moments, contrary to the experimental observation [26].

Very recently, calculations using the adiabatic time-dependent Hartree-Fock-Bobolyubov approach with the Skyrme interaction SIII have been used to generate both the potential energy and mass parameters for the Bohr Hamiltonian [32]. The potential energy surfaces for the  $^{106-116}\text{Cd}$  isotopes, in general, have a minimum with  $\beta$  near 0.2, and are prolate with  $\gamma$  close to zero, although there is a weak  $\gamma$  dependence [32]. Non-zero quadrupole moments are calculated which are typically somewhat larger than the experimental values.

It has been pointed out [11] that the properties of the  $0_4^+$  levels in the  $^{110-116}\text{Cd}$  isotopes, their “V-shaped” excitation-energy pattern as a function of neutron number, and their strongly favored decay to the  $2_3^+(i)$  intruder band members, are consistent with their assignments as excitations built on the intruder band. The very-low energy relative to the intruder band head, however, lying below the position of the first  $4^+$  intruder state and approaching the first  $2^+$  intruder level, is difficult to reproduce as a typical collective-type excitation that might be built on the intruder  $0^+$  state. It seems possible that the 2079-keV state is a  $4p - 6h$  proton excitation. It would be expected that this configuration would have an even more deformed shape than the  $2p - 4h$  excitation and should thus act as a band head for a rotational-like band. Additional detailed spectroscopy is required to seek the weak in-band decay branches needed to identify such possible band members.

#### IV. CONCLUSIONS

Results from a high-statistics  $^{110}\text{In}$   $\beta^+$ /EC-decay experiment, combined with a reanalysis of  $(n, n'\gamma)$  data including level lifetimes, has resulted in the establishment of stringent upper limits on unobserved branches and of more precise  $B(E2)$  values than were previously available. It is found that, generally, the vibrational-phonon and intruder states do not have enhanced  $E2$  transitions connecting them, apart from the  $0^+$  intruder band head and the  $6_1^+$  member of the ground-state band. Thus, there is no evidence for the strong mixing of the intruder and non-intruder configurations except for the ground-state band. The rejection of the strong-mixing scenario reveals that the non-intruder states are not vibrational, but the decay pattern is strongly suggestive of a  $\gamma$ -soft, or  $O(6)$ -type nucleus. The existence of the proton  $4p - 6h$  excitation is speculated upon.

## ACKNOWLEDGMENTS

The assistance of Drs. F. Corminboeuf and L. Genilloud in the collection of the  $(n, n'\gamma)$  data is gratefully acknowledged. This work was supported in part by the Natural Sciences and Engineering Research Council (Canada), TRIUMF through the National Research Council (Canada), by the U.S. National Science Foundation under Grant No. PHY-0956310, and by the DFG cluster of excellence ‘Origin and Structure of the Universe’.

- 
- [1] F.K. McGowan, R.L. Robinson, P.H. Stelson, and J.L.C. Ford, Jr., Nucl. Phys. **66**, 97 (1965).
- [2] P.D. Barnes, J.R. Comfort, and C.K. Bockelman, Phys. Rev. **155**, 1319 (1965).
- [3] J. Kern, P.E. Garrett, J. Jolie, and H. Lehmann, Nucl. Phys. **A593**, 21 (1995).
- [4] B.L. Cohen and R.E. Price, Phys. Rev. **118**, 1582 (1960).
- [5] R.A. Meyer and L. Peker, Z. Phys. A **283**, 379 (1997).
- [6] K. Heyde, P. Van Isacker, M. Waroquier, G. Wenes, and M. Sambataro, Phys. Rev **C25**, 3160 (1982).
- [7] H.W. Fielding R.E. Anderson, C.D. Zafiratos, D.A. Lind, F.E. Cecil, H.H. Weiman, and W.P. Alford, Nucl. Phys. **A281**, 389 (1977).
- [8] Data extracted from the National Nuclear Data Center, [www.nndc.bnl.gov](http://www.nndc.bnl.gov).
- [9] M. Déléze, S. Drissi, J. Kern, P.A. Tercier, J.-P. Vorlet, J. Rikovska, T. Otsuka, S. Judge, and A. Williams, Nucl. Phys. **A551**, 269 (1993).
- [10] M. Déléze, S. Drissi, J. Jolie, J. Kern, and J.-P. Vorlet, Nucl. Phys. **A554**, 1 (1993).
- [11] P.E. Garrett, K.L. Green, and J.L. Wood, Phys. Rev. C **78**, 044307 (2008).
- [12] P.E. Garrett, K.L. Green, H. Lehmann, J. Jolie, C.A. McGrath, M. Yeh, and S.W. Yates, Phys. Rev. C **75**, 054310 (2007).
- [13] D. Bandyopadhyay, S.R. Leshner, C. Fransen, N. Boukharouba, P.E. Garrett, K.L. Green, M.T. McEllistrem, and S.W. Yates, Phys. Rev. C **76**, 054308 (2007).
- [14] M. Kadi, N. Warr, P.E. Garrett, J. Jolie, and S.W. Yates, Phys. Rev. C **68**, 031306(R) (2003).
- [15] J.C. Batchelder, J.L. Wood, P.E. Garrett, K.L. Green, K.P. Rykaczewski, J.-C. Bilheux, C.R. Bingham, H.K. Carter, D. Fong, R. Grzywacz, J.H. Hamilton, D.J. Hartley, J.K. Hwang, W. Krolas, W.D. Kulp, Y. Larochelle, A. Piechaczek, A.V. Ramayya, E.H. Spejewski, D.W. Stracener, M.N. Tantawy, J.A. Winger, and E.F. Zganjar, Phys. Rev. C **80**, 054318 (2009).
- [16] P.E. Garrett and J.L. Wood, J. Phys. G **37**, 064028 (2010); corrigendum *ibid.*, 069701.
- [17] P.E. Garrett, A. Andreyev, R.A.E. Austin, G.C. Ball, D. Bandyopadhyay, J.A. Becker, A.J. Boston, H.C. Boston, R.S. Chakrawarthy, R. Churchman, D. Cline, R.J. Cooper, D. Cross, D. Dashdorj, G.A. Demand, M.R. Dimmock, T. Drake, P. Finlay, K. Gagnon, A.T. Gallant, K.L. Green, A.N. Grint, G.F. Grinyer, G. Hackman, L.J. Harkness, A.B. Hayes, R. Kanungo, W.D. Kulp, K.G. Leach, G. Lee, J.R. Leslie, R. Maharaj, J.-P. Martin, C. Mattoon, W.J.

- Mills, A.C. Morton, L. Nelson, O. Newman, P.J. Nolan, E. Padilla-Rodal, C.J. Pearson, A.A. Phillips, M. Porter-Peden, J.J. Ressler, C. Ruiz, F. Sarazin, M.A. Schumaker, D.P. Scraggs, M.D. Strange, M. Subramanian, C.E. Svensson, J.C. Waddington, J. Wan, A. Whitbeck, S.J. Williams, J.L. Wood, J.C. Wong, C.Y. Wu, and E.F. Zganjar, *Acta Phys. Polonica B* **38**, 1169 (2007).
- [18] F. Corminboeuf, T. B. Brown, L. Genilloud, C. D. Hannant, J. Jolie, J. Kern, N. Warr, and S. W. Yates, *Phys. Rev. C* **63**, 014305 (2000).
- [19] F. Corminboeuf, T. B. Brown, L. Genilloud, C. D. Hannant, J. Jolie, J. Kern, N. Warr, and S. W. Yates, *Phys. Rev. Lett.* **84**, 4060 (2000).
- [20] P.E. Garrett *et al.*, unpublished.
- [21] W.D. Kulp, J.L. Wood, J.M. Allmond, J. Eimer, D. Furse, K.S. Krane, J. Loats, P. Schmelzenbach, C.J. Stapels, R.-M. Larimer, E.B. Norman, A. Piechaczek, *Phys. Rev. C* **76**, 034319 (2007).
- [22] L.A. Currie, *Anal. Chem.* **40**, 586 (1968).
- [23] J. Kern, A. Bruder, S. Drissi, V.A. Ionescu, and D. Kusnezov, *Nucl. Phys.* **A512**, 1 (1990).
- [24] J. Kumpulainen, R. Julin, J. Kantele, A. Passoja, W.H. Trzaska, E. Verho, J. Väärämäki, D. Cutoiu, and M. Ivascu, *Phys. Rev. C* **45**, 640 (1992).
- [25] M. Bertschy, S. Drissi, P.E. Garrett, J. Jolie, J. Kern, S.J. Mannanal, J.-P. Vorlet, N. Warr, and J. Suhonen, *Phys. Rev.* **C51**, 103 (1995).
- [26] G. Gurdal and F.G. Kondev, *Nucl. Data Sheets* **113**, 1315 (2012).
- [27] Yu.N. Lobach, A.D. Efimov, and A.A. Pasternak, *Eur. Phys. J. A* **6**, 131 (1999).
- [28] K.L. Green, P.E. Garrett, R.A.E. Austin, G.C. Ball, D.S. Bandyopadhyay, S. Colosimo, D. Cross, G.A. Demand, G.F. Grinyer, G. Hackman, W.D. Kulp, K.G. Leach, A.C. Morton, C.J. Pearson, A.A. Phillips, M.A. Schumaker, C.E. Svensson, J. Wong, J.L. Wood, and S.W. Yates, *Phys. Rev. C* **80**, 032502 (2009).
- [29] J. Jolie and H. Lehmann, *Phys. Lett.* **B342**, 1 (1995).
- [30] J.L. Wood, E.F. Zganjar, C. de Coster, and K. Heyde, *Nucl. Phys.* **A651**, 323 (1999).
- [31] L. Wilets and M. Jean, *Phys. Rev.* **102**, 778 (1955).
- [32] L. Próchniak, P. Quentin, and M. Imadalou, *Int. J. Mod. Phys. E* **21**, 1250036 (2012).